Characterization of the aerosol produced by infrared femtosecond laser ablation of polyacrylamide gels for the sensitive inductively coupled plasma mass spectrometry detection of selenoproteins

F. Claverie, Christophe Pécheyran, Sandra Mounicou, G. Ballihaut, B. Fernandez, Joel Alexis, Ryszard Lobinski, Olivier François Xavier Donard

Characterization of the aerosol produced by infrared femtosecond laser ablation of polyacrylamide gels for the sensitive inductively coupled plasma mass spectrometry detection of selenoproteins

Fanny Claverie [a,b], Christophe Pécheyran [a,*], Sandra Mounicou [a], Guillaume Ballihaut [a,c], Beatriz Fernandez [a], Joël Alexis [d], Ryszard Lobinski [a], Olivier F.X. Donard [a]

[a] Laboratoire de Chimie Analytique Bio-Inorganique et Environnement, Institut Pluridisciplinaire de Recherche sur l'Environnement et les Matériaux, UMR 5254 CNRS- Université de Pau et des Pays de l'Adour, Hélioparc Pau-Pyrénées, 2 Avenue du Président Angot, 64053 Pau Cedex 9, France
[b] Novalase SA, Z.I de la Briqueterie, 6 Impasse du bois de la Grange, 33610 Canéjan, France
[c] Laboratoire d'Ecologie Moléculaire (Microbiologie), UMR 5254 CNRS- Université de Pau et des Pays de l'Adour, avenue de l'Université, B.P. 1155, F-64013 Pau, France
[d] Laboratoire Génie de Production, Ecole Nationale d'Ingénieurs de Tarbes, 47 avenue d'Azereix BP 1629, 65016 Tarbes, France

ARTICLE INFO

Article history:
Received 24 October 2008
Accepted 27 May 2009
Available online 8 June 2009

Keywords:
Femtosecond laser ablation
Aerosol characterization
Polyacrylamide gel
ICPMS

ABSTRACT

A 2D high repetition rate femtosecond laser ablation strategy (2-mm wide lane) previously developed for the detection of selenoproteins in gel electrophoresis by inductively coupled plasma mass spectrometry was found to increase signal sensitivity by a factor of 40 compared to conventional nanosecond ablation (0.12-mm wide lane) [G. Ballihaut, F. Claverie, C. Pécheyran, S. Mounicou, R. Grimaud and R. Lobinski, Sensitive Detection of Selenoproteins in Gel Electrophoresis by High Repetition Rate Femtosecond Laser Ablation-Inductively Coupled Plasma Mass Spectrometry, Anal. Chem. 79 (2007) 6874–6880]. Such improvement couldn't be explained solely by the difference of amount of material ablated, and then, was attributed to the aerosol properties. In order to validate this hypothesis, the characterization of the aerosol produced by nanosecond and high repetition rate femtosecond laser ablation of polyacrylamide gels was investigated. Our 2D high repetition rate femtosecond laser ablation strategy of 2-mm wide lane was found to produce aerosols of similar particle size distribution compared to nanosecond laser ablation of 0.12-mm wide lane, with 38% mass of particles <1 μm. However, at high repetition rate, when the ablated surface was reduced, the particle size distribution was shifted toward thinner particle diameter (up to 77% for a 0.12-mm wide lane at 285 μm depth). Meanwhile, scanning electron microscopy was employed to visualize the morphology of the aerosol. In the case of larger ablation, the fine particles ejected from the sample were found to form agglomerates due to higher ablation rate and then higher collision probability. Additionally, investigations of the plasma temperature changes during the ablation demonstrated that the introduction of such amount of polyacrylamide gel particles had very limited impact on the ICP source (ΔT~25 ± 5 K). This suggests that the cohesion forces between the thin particles composing these large aggregates were weak enough to have negligible impact on the ICPMS detection.

1. Introduction

The detection of metals and metalloids in proteins is of growing concern in biochemical, toxicological and pharmacological sciences [1]. However, their detection still remains a challenge due to the low concentration levels that they exhibit in proteins. Traditionally, the sensitive detection of heteroatoms in proteins separated by gel electrophoresis was performed with autoradiography [2,3]. However, this technique is limited by several drawbacks such as the use of radioactive isotopes and the non-applicability to human samples. Allowing its unique features, there was an increased interest in laser ablation inductively coupled plasma mass spectrometry (LA-ICPMS) in the growing proteomic field, and by the end of the 90s, McLeod et al. [4] proposed the scanning of gels by laser ablation (LA). Since then, studies on different element containing proteins after separation by gel electrophoresis and detection by ICPMS after LA sampling have been reported [2]. However this technique still suffers from some limited analytical performances which are mainly due to the small amount of protein effectively sampled for the analysis.

Previously [5], we developed a sensitive method based on the combination of high repetition rate femtosecond (fs) LA-ICPMS with a fast scanning beam device for the detection of selenoproteins in gel electrophoresis. This technique allows the detection of the selenoproteins in gel electrophoresis at the low-femtomolar levels. Compared to a conventional nanosecond (ns) laser ablating 120-μm wide lanes, the signal sensitivity was drastically improved by a factor of 40 by ablating quasi-instantaneously 2-mm wide lanes of gels. However, the mass of

* Corresponding author. Tel.: +33 559 407 757; fax: +33 559 407 781.
E-mail address: Christophe.pecheyran@univ-pau.fr (C. Pécheyran).

material sampled was only 27 times higher than the mass sampled with the ns laser. Therefore the amount of gel ablated cannot exclusively explained the enhanced sensitivity obtained by the femtosecond 2-mm wide lane ablation. Such improvement could be assigned to the nature of the aerosol produced by the shorter fs pulses with a better particle distribution in a nanometer range [6,7]. Consequently, the aerosols produced by LA should be investigated in detail to confirm this hypothesis and evaluate the direct effect of fs laser pulses on aerosol composition and signal sensitivity.

The investigation of the aerosol is of great interest to improve the quality of the signal and/or determine the existing particle fractionation. Parameters such as transport efficiency, stability, sensitivity and fractionation have been widely studied in relation with particle size distribution [8–12] and particle dispersion [13]. Separation devices, filters, impactors and stabilizers were also investigated to remove bigger particles and, thus, yield precise and stoichiometric measurements [14–18] but this process is accompanied by a great loss of the signal. Therefore, recent studies are more focused on the formation of a fine aerosol by using well chosen laser parameters.

Indeed, the formation of the aerosol depends on the laser process itself which is governed by the sample properties and the laser characteristics. Furthermore, depending on the sample studied, key parameters can appear. The wavelength has to be associated with the sample absorbance, as it determines the amount of molten micron-sized spherical particles produced by nanosecond laser ablation [14,19,20]. The fluence has to be adapted to the sample studied, particularly for metals whose high conductivity induces splashing of large droplets at high energy density, and non-stoichiometric aerosol at too low energy density [10,19]. Finally, pulse duration influences the laser-material interaction. Indeed, short pulses below 1 ps have been demonstrated to provide less thermal effects and less material damages compared to nanosecond pulses: the occurrence of melting effects and cracks is drastically reduced and smaller particles are produced [21,22]. Furthermore, it results in a better vaporization within the ICP and a minimized fractionation [11,23]. The generation of these different particles is complex and not clearly understood yet. Hergenröder [24] has recently reviewed the particle formation processes highlighting the numerous and complex mechanisms which can take place during LA. Three modes of material removal can be distinguished: atomization and subsequent gas-to-particle conversion, liquid droplet expulsion, and solid material ejection.

However, materials expelled are also modified from the ablation cell to their transfer into the ICP. Papers related to transport processes [25–29] showed that using helium as carrier gas permits a better transport efficiency whereas the geometry of the ablation cell influences only the dispersion of the aerosol. Moreover, the transport tube has to be as short as possible to avoid the deposition of particles which could be source of fractionation [30]. The visualization of the aerosol inside the ablation cell and the transport tube was recently studied by Koch et al. [13,31,32] in order to understand the behavior of the aerosol immediately after the impact of the laser and during the transport. Such studies revealed that femtosecond laser ablation (fs-LA) generally induces a homogenously distributed aerosol on turbulent flow and a more dynamic expansion perpendicular to the sample surface. Nevertheless, even if the use of fs pulses results in a more dispersive aerosol, aggregates are formed as in the case of ns pulses. Different shapes of agglomerates have been reported depending on the sample material: cotton-like for CaF_2 and linear-agglomerate for metals and silicates [19]. The cohesion of these agglomerates can be strong or weak which leads Gonzalez et al. [33,34] to define agglomerates as “hard” or “soft” respectively. Despite the formation of these aggregates, the transported mass was at least 77% for fs-LA [29], which means that agglomerates can be transported until the ICP source.

Finally, laser-produced aerosols are vaporized in the ICP. The plasma has to atomize nano-particles as well as agglomerates which could present severe limitations when too large or too “hard agglomerates” are produced. Moreover, the temperature of the plasma can be affected by a mass overloading which results in preferential atomisation/ionisation of elements [8] and/ or in a decrease of intensity ratios such as Cu/Ca, Zn/Ca, Cd/Ca, and Pb/Ca [35]. Therefore, it can be stated that ICPMS signal is dependent on the aerosol composition: particles not completely atomized and/or important mass loading induce fractionation, large particles induce signal fluctuations and, finally, smaller particles are better transported, atomised and ionised which in turn induce better sensitivity, signal stability and accurate results.

Therefore the characterization of an aerosol includes particle size distribution measurements and morphology. Both have been widely studied during the last years for a broad range of solid materials such as glasses [34,36], metals [33,37], CaF_2 and calcite [17]. Nevertheless, even if some interesting applications are based on the analysis of proteins included in gels, to our knowledge, complex matrices as polyacrylamide samples have not been studied so far as laser-produced aerosol for LA-ICPMS analyses. Therefore, the aim of this study was to investigate the nature of the particles produced by laser ablation of polyacrylamide gels in order to explain the enhancement factor of 40 found between the nanosecond and femtosecond laser ablation [5]. Particle size distribution of aerosols produced by ns- and fs-LA was determined using low-pressure impaction, and morphology of collected aerosol particles was visualized by scanning electron microscopy (SEM). Additionally, the plasma temperature changes were determined to investigate possible plasma loading effects on the ICP.

2. Experimental section

2.1. Instrumentation

2.1.1. Laser ablation-ICPMS systems

Two laser ablation systems were used in order to compare ablations of polyacrylamide gels performed at nanosecond and femtosecond pulses.

A unique femtosecond laser ablation device (Novalase SA — France) fitted with a diode-pumped KGW-Yb laser was employed. It delivers 360 fs pulses at an IR-wavelength of 1030 nm and operates at high repetition rate from 1 Hz to 10 kHz with a low energy of 0.1 to 100 μJ at the sample surface. In these conditions, the beam size focused at the sample surface is 17 μm ($1/e^2$). A galvanometric scanning beam device allows the laser beam (focused on a 50 mm objective) to rapidly move (up to 280 mm s^{-1}) with a high repositioning precision (<1 μm). Further, the ablation cell (10 cm^3) is mounted on a motorised XY stages permitting the sample positioning. The software can synchronise the sample (XY stages) and the laser beam (scanner) movements to perform complex trajectories. The combination of the high repetition rate and the fast scanning beam allows ablating much larger surface than the nominal 17 μm spot size, quasi-instantaneously at the detection time scale of a quadrupole ICPMS [5,38–40]. The design features of the laser are described elsewhere [38].

A UV 266-nm nanosecond (8 ns pulses) laser ablation system model LSX-100 (Cetac, Omaha, NE) operated at 20 Hz and 1.1 mJ was used as a reference system. A 5 cm diameter (30 cm^3) ablation cell was used. The lane width obtained at the selected experimental conditions was of 120 μm.

The ICPMS measurements were performed with the Agilent model 7500 cs in the operating collision cell mode, which was daily optimized with Xe gas. Helium was chosen as carrier gas in the ablation cell and xenon was added by a Y connection at the outlet of the ablation cell as external standard in order to check for ICPMS plasma instability. Due to the high amount of polyacrylamide gel introduced into the plasma, oxygen was added to the Ar blend flow rate in order to prevent carbon deposition on the cones. Oxygen was added for nanosecond laser ablation too in the same proportion. Experience showed that oxygen was particularly required when large femtosecond laser ablation rates were used since carbon deposition, as well as sensitivity

and reproducibility drifts were observed when insufficient oxygen flow rate was added to the plasma. Because of the oxygen addition, and due to potential formation of selenium oxide, the optimization was also focused on the oxide level ($^{156}CeO/^{140}Ce$) to be below 5%. A three-inlet interface was used to mix the laser-produced aerosol, and the argon carrier gas containing 5% v/v O_2. A 1.5 mm-i.d torch and a platinum sampler and skimmer cones were used. This configuration was used throughout this study except for the determination of the plasma temperature changes where an ultrasonic nebuliser (USN U5000AT+, Cetac) was connected to produce a quasi-dry aerosol permitting the introduction of gallium and germanium. Operating conditions of the ICPMS and characteristics of the laser ablation systems are summarised in Table 1.

2.1.2. Low-pressure impaction

A commercial 13 detection stages impactor (ELPI — Ecomesure — France) was connected to the laser systems in order to measure the particle size distribution of the aerosol carried by the helium stream. The low-pressure impaction system is designed for the collection of airborne particles ranging from 7 nm to 10 μm aerodynamic diameter in air.

The geometry of the ELPI imposes a total inlet flow of 10 L min^{-1} of air in order to ensure an accurate particle size distribution measurement. However, taking into account that He-transported particles are mixed with an argon flow at the entrance of the ICP torch when the laser is coupled to the ICPMS, an argon flow, instead of air flow, was used to maintain a total flow rate (He + Ar) of 10 L min^{-1}. Argon was chosen in order to simulate as well as possible the gas property conditions prevailing in the entrance of the torch. As a consequence, Ar viscosity and molecular weight were selected in the ELPI software to recalculate the actual aerodynamic diameter for each stage (10 nm, 36 nm, 69 nm, 115 nm, 185 nm, 303 nm, 436 nm, 691 nm, 1.06 μm, 1.777 μm, 2.65 μm, 4.417 μm, and 10.937 μm). Moreover, taking into account the unknown density of the gels, mass values presented in the following sections were only used as indicative values for comparison between different ablations. In addition, it is possible to record in real time particle size distribution during the ablation. An integration time of 1 s was selected for this purpose providing a complete particle size distribution each second.

2.1.3. Scanning electron microscopy

The laser generated aerosol particles were collected on polycarbonate membrane filters with a pore size of 200 nm (Whatman nucleopore), which were placed approximately 1 m behind the ablation cell. Though not provided by the manufacturer, the collection efficiency of these filters was found to be 100% since no signal could be detected when the filters were placed online with the ICPMS. Next, these membranes were glued on SEM-mounts using a conducting double carbon tape and metallised during 4 min with palladium to remove artefacts. Such metal coating was performed with a SEM coating E5000 (Polaron Equipment LTD) at intensity levels between 16 and 18 mA under nitrogen atmosphere (2.37×10^{-4} atm). The scanning electron microscope used was a SEM Field Emission Scanning JEOL 7000F (JEOL Ltd, Japan) operated at 5 kV.

Table 1
Operating conditions of the ICPMS and characteristics of the ablation systems.

ICP-MS	Agilent model 7500cs	
Argon gas	0.81 L min^{-1}	
O_2	40 mL min^{-1} (5% v/v argon blend)	
Collision cell gas (H_2)	3.4 mL min^{-1}	
RF power	1500 W	
Torch injector	1.5 mm	
Cones	Pt	
Isotopes[a]	^{77}Se, ^{78}Se, ^{80}Se, ^{82}Se, ^{69}Ga, ^{71}Ga, ^{70}Ge, ^{72}Ge, ^{74}Ge, ^{124}Xe, and ^{126}Xe	
Laser ablation system	ALFAMET Novalase SA	LSX-100 Cetac
Laser type	KGW-Yb	Nd-YAG
Wavelength	1030 nm	266 nm
Pulse duration	360 fs	8 ns
Repetition rate	1–10 000 Hz	20 Hz
Pulse energy	<100 μJ $pulse^{-1}$	1.1 mJ $pulse^{-1}$
Crater diameter	17 μm	120 μm
Carrier gas flow rate (He)	700 mL min^{-1}	700 mL min^{-1}

[a] Gallium and germanium were analyzed only for the investigation of the plasma loading.

2.2. Protocol

2.2.1. Preparation of polyacrylamide gel samples

The selenoprotein glutathione peroxidase (4.2 mg, 123 units mg^{-1} of solid and 673 unit mg^{-1} of protein) was purchased from Sigma-Aldrich (St-Quentin Fallavier, France) and solubilized with 2 mL of 50 mM Tris–HCl, and 1 mM Tris(2-carboxyethyl)phosphine hydrochloride (TCEP) pH 9. The sample was divided into 5 aliquots of 400 μL each and kept frozen at −20 C until utilization. One aliquot was partially dedicated to the determination of total selenium by ICPMS and was found to contain 843.5 ng Se mL^{-1} by means of standard addition method. The other part of this aliquot was analyzed by size exclusion chromatography coupled to ICPMS under experimental conditions described elsewhere [41] to determine the proteinous selenium which was assessed to 90%.

The four other aliquots were used for SDS–PAGE allowing the preparation of (1) a gel sample containing a unique lane with a wide selenoprotein band to perform comparative measurements and (2) a gel sample with different selenoprotein concentrations to realize a calibration curve. Further details of the reagents and the experimental procedure used to perform the gel electrophoresis are described in a previous publication [5]. After electrophoresis, the gel was rinsed, stained with Coomassie Blue, destained and vacuum-dryed on a filter paper finalizing the preparation of the sample that is now ready to be ablated.

2.2.2. Nebulization solution

A solution containing 0.1 μg L^{-1} of germanium and gallium was prepared from CCS5 solution (Inorganic Ventures, Lakewood, NJ, USA) and a gallium solution (Sigma-Aldrich). Ultra-pure water was obtained from a Milli-Q system (18.2 MW, Millipore, USA) and ultrapure nitric acid (Ultrex) was purchased from J. T. Baker (Phillipsburg, NJ, USA). This nebulization solution was used for the study of the plasma temperature changes.

2.2.3. Ablation strategies

The main objective of the present work was to explain the enhanced sensitivity obtained by using the 2-mm wide lane femtosecond laser ablation strategy at 10 kHz [5] compared to smaller lane width generally produced by conventional nanosecond laser ablation (typically 0.12 mm in our previous work [5]). These ablation strategies are denoted as the “reference femtosecond ablation” and the “reference nanosecond ablation” all along this paper.

The nanosecond laser system used in this study (CETAC LSX 100) allows only the movement of the sample while the laser beam is kept in the same position. In contrast, the femtosecond laser device (Alfamet Novalase) permits to realise complex trajectories in two dimensions (2D), by moving at the same time the laser beam and the sample.

By combining these 2D ablation trajectories (using the fast laser beam movement together with the sample movement) with the high repetition rate of the laser (up to 10 kHz) it is then possible to increase considerably the amount of ablated material introduced into the ICPMS compared to conventional nanosecond laser ablation. As it can be seen from Table 2, the 2D ablation consisted in a back-and-forth vertical movement of the laser beam, combined with the horizontal

Table 2
Ablation parameters and resulted depth and ablation rates calculated for the highest fluence value of 17 J cm^{-2} for femtosecond laser ablation and 19 J cm^{-2} for nanosecond laser ablation.

	Laser	Width lane (mm)	Repetition rate (Hz)	Scan speed rate (mm s^{-1})	Fluence (J cm^{-2})	Depth (μm)	Ablation rate (mm^3 s^{-1})	Scheme of the ablation
Reference ablation	Nanosecond	0.12	20		19	70	2.64×10^{-4}	Laser beam fixed Width lane Movement of the gel V_{stage} = 60 μm s^{-1}
Same depth	Femtosecond	2	10000	100	17, 8.6, 4.3 and 2.2	75	6.98×10^{-3}	Movement of the laser beam V_{scan} Width lane Movement of the gel V_{stage} = 50 μm s^{-1}
		0.12	600	6	17	83	3.93×10^{-4}	
		0.5	2500	25		83	1.82×10^{-3}	
		1	5000	50	17, 8.6, 4.3 and 2.2	91	4.06×10^{-3}	
		1.5	7500	75	17	88	6.15×10^{-3}	
At high repetition rate	Femtosecond	0.12	10000	100	17	285	1.10×10^{-3}	
		0.5		100		203	3.76×10^{-3}	
		1		100		117	5.10×10^{-3}	
		1.5		100		88	5.80×10^{-3}	

displacement of the sample. Changing the ablation parameters (fluence, speed of the laser beam, sample movement and repetition rate) allowed the control of the amount of gel ablated.

The "reference nanosecond ablation" resulted in a 0.12 mm × 0.07 mm (Width × depth) lane. As the femtosecond laser system allows controlling the depth of ablation by adjusting the number of shots per surface unit, the same amount of material (0.12 mm × 0.07 mm (width × depth)) was ablated with the femtosecond laser in order to study the impact of shorter pulses. Additional lane widths (0.5, 1, 1.5 and 2 mm) were also ablated while keeping the same resulting depth (0.07 mm) in order to study the impact of the amount of particles introduced into the ICP. It consists in modifying the repetition rate (from 600 Hz to 10 kHz) and the scanner speed (from 6 mm s^{-1} to 100 mm s^{-1}) in order to obtain the same pulse overlapping (pulse density per surface unit) which results in the same ablation depth.

The "reference femtosecond ablation" corresponds to a 2-mm wide lane performed at high repetition rate (10 kHz). In order to study the aerosol generation processes at this repetition rate, 0.12, 0.5, 1, 1.5 and 2-mm wide lanes were ablated while keeping the same scanning speed in each case (100 mm s^{-1}). The ablation depths obtained ranged from 75 μm to 285 μm depending on the width of the lane.

Finally, two ablation strategies (the "reference femtosecond ablation" and a 1-mm wide lane ablation at 5 kHz) were realised at 4 different fluence values in order to evaluate the impact of this parameter on the aerosol properties.

The depth and the ablation rate were calculated owing to the topography of the ablations which was performed with an optical surface profilometer Micromesure CHR150 (STIL society, France).

3. Results and discussion

3.1. Particle size distribution of the laser generated aerosol

Particle size measurements have been widely studied to understand the impact of laser parameters on the ICPMS signal. The influence of the laser wavelength on fractionation for different samples [20,27] as well as the influence of the carrier gas [27], the fluence [36,37] and the pulse duration [11,37] were recently reported and related to the particle sizes of the aerosol. Different techniques have been evaluated by Kuhn et al. [42], for this purpose and particle impaction was found to be a suitable technique for aerosol studies thanks to its working range which is large enough for the analysis of this kind of mixed aerosols.

3.1.1. Nanosecond versus femtosecond ablation

First, the particle size distribution of the generated aerosol was measured after nanosecond and femtosecond laser ablation to compare the analytical performances of both systems for the analysis of polyacrylamide gels. An identical ablation lane was realized with both lasers taking into account the depth and the width of the scan (in the order of 80 μm and 0.12 mm, respectively). Furthermore, femtosecond analysis was performed at 17 J cm^{-2} with a repetition rate of 600 Hz and a scanner speed of 6 mm s^{-1} in order to draw a 0.12-mm wide lane with the same laser pulses overlapping and at the same fluence than the reference femtosecond ablation. Fig. 1a and b shows respectively the particle size distribution in mass percentage of the laser-produced aerosol after the nano- and femtosecond laser ablation of polyacrylamide gels. Shorter pulses were found to produce finer particles though in a limited extent showing a mass percentage of nanometric particles (<1 μm) of 44 ± 4% in comparison with 38 ± 3% for the nanosecond laser ablation. Such effect demonstrated only a slight positive impact of the femtosecond pulses on the aerosol formation which cannot explain the great improvement factor of sensitivity reported in our previous paper [5]. Moreover, Fig. 1c represents the particle size distribution obtained for the reference femtosecond ablation and, as it can be observed, the mass percentage of nanometer

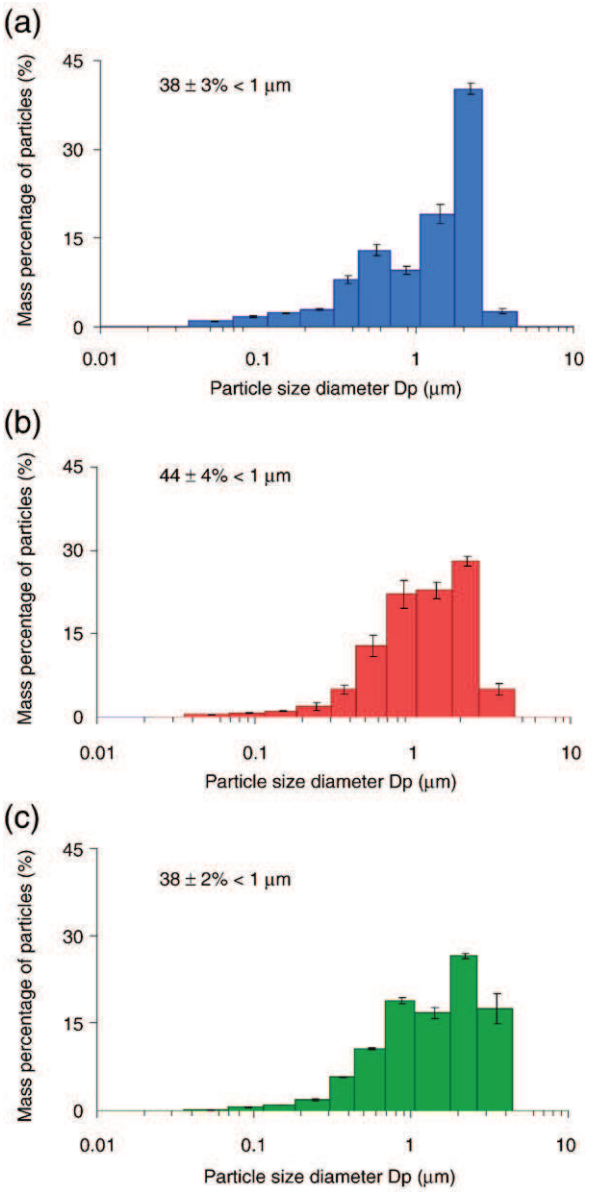

Fig. 1. Particle size distribution in mass percentage of the laser generated aerosol of polyacrylamide gels. The uncertainty (standard deviation) was calculated from 3 replicates. (a) Nanosecond laser ablation at 20 Hz (reference nanosecond ablation: 0.12-mm wide lane). (b) Femtosecond laser ablation at 600 Hz (0.12-mm wide lane). (c) Femtosecond laser ablation at 10 kHz (reference femtosecond ablation: 2-mm wide lane).

particles was quite similar (38%) than for the reference nanosecond ablation (Fig. 1a).

The expansion of the ablation lane width from 0.12 to 2 mm in femtosecond ablation (keeping the same crater overlapping, depth, and fluence) produced a slight mass distribution shift toward thicker particles (from 44% to 38% of nano-particles). The calculated ablation rate was 3.93×10^{-4} mm^3 s^{-1} and 6.98×10^{-3} mm^3 s^{-1} for the 0.12-mm and the 2-mm wide lanes respectively, which represents an 18 fold increase in the mean particles density into the cell. Such a high particle density prevailing into the cell may favor more collisions and aggregation of nano-particles into micro-particles and it was confirmed by the particle size distribution in number as shown in Fig. 2.

These results underline the importance of investigating more in detail the morphology of the laser generated particles in order to understand the complex processes involved in the aerosol formation and transport. It is known from brass studies that IR femtosecond

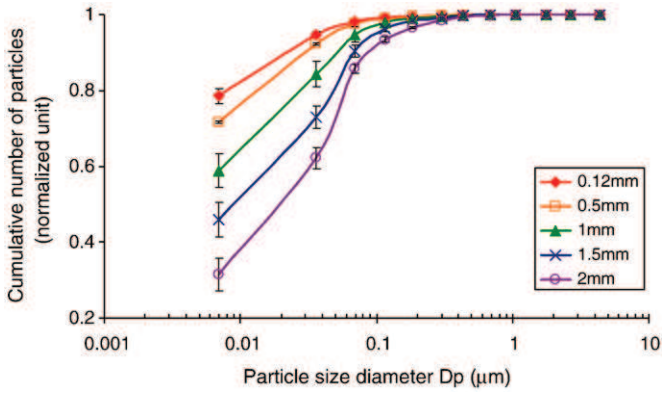

Fig. 2. Cumulative particle size distribution, normalized to unit, for ablations at the same depth. The uncertainty (standard deviation) was calculated from 3 replicates.

pulses produces smaller particles than nanosecond pulses [22,37]. Previous studies by scanning electron microscopy revealed that the aerosols produced by fs laser pulses were constituted of smaller particles and larger agglomerates compared to nanosecond laser ablation [11,23,33,34,43]. This will be investigated in our case in a following section.

3.1.2. Effect of the high repetition rate

A particularity of the laser system used in this study is its high repetition rate of 10 kHz compared to conventional laser system working from 1 to 100 Hz. In order to study in detail the impact of this parameter, all ablations were performed at 10 kHz changing the ablated wide lane from 0.12 to 2 mm. The speed of the scanner was kept at 100 mm s^{-1} and the sample movement at 50 µm s^{-1} (see Table 2). Under these conditions, the number (N) of back-and-forth cycles made by the scanner during a given period of time is inversely proportional to the ablation width. Hence, when the ablation width decreases, N increases as well as the number of shots per surface unit resulting in a deeper ablation lane ranging from 0.075 mm for the 2-mm wide lane to 0.285 mm for the 0.12-mm wide lane. The mass percentage of particles under 1 µm for ablation width ranging from 0.12 mm to 2 mm is presented in Fig. 3. Up to 77% of the particles were below 1 µm when ablating a 0.12×0.285 mm^2 (width × depth) lane which contrasts with the 2×0.075 mm^2 (width × depth) lane where 38% of the particles were below 1 µm. Moreover, this drop of nano-particles showed a linear trend with the ablation rate. These results clearly indicated that the particle size was shifted toward finer particles when the ablation rate decreased and the depth of the lane increased.

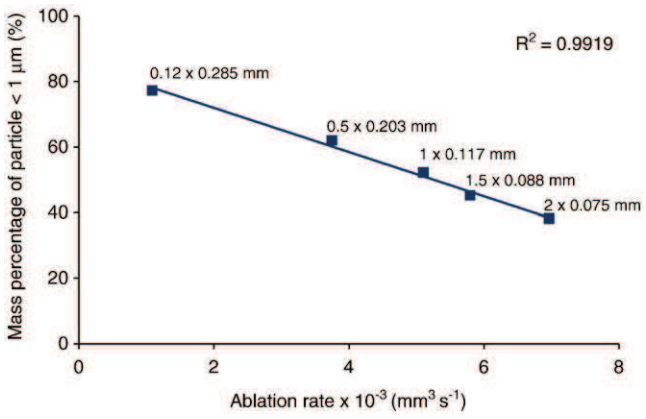

Fig. 3. Evolution of the mass percentage of particles below 1 µm for ablations at 10 kHz. Each point represents "a width × a depth" ablation.

At least three phenomena could explain these results. First, as it has been demonstrated by Guillong et al. [14], scanning mode ablation produces larger particles in comparison to the crater mode because of its occurrence at the sample surface (using the crater mode, the particle size diameter decreased with the increasing of the depth). However, though raster ablation mode was used in our experiments, the combination of the high repetition rate and the scanning beam device permitted to go deeper in the gels and, therefore, to produce smaller particles. Further, after electrophoresis, the gel is dried on a piece of paper which could be ablated with the smallest and then the deepest ablation lanes. By visualizing the edge of the gels, the thickness was evaluated around 200 µm and, therefore, it is possible that a part of the aerosol particles produced by an ablation lane of 0.12 mm at high repetition rate was coming from the paper support. However, the point corresponding to the 0.12 mm ablation lane where small amount of paper has been ablated fits perfectly with the slope presented in Fig. 3 showing that the influence of the paper is of limited importance in these conditions.

On the other hand, the ablation rate plays an important role on the composition of the laser-produced aerosol. Indeed, when a large amount of gel is ablated, the probability of collision and, thus, of aggregation increases. The thin particles ejected from the sample can then more easily stick to each other to form bigger agglomerates during laser ablation processes and transport. Fig. 4 shows the evolution of the number of particles above and below 1 µm recorded in real time during the ablation of 2×0.075 mm^2 lane. The number of nanoparticles (black line) dropped drastically with time during the ablation while the number of micrometric particles increased (dashed line). This demonstrates that the accumulation of particles inside the ablation cell shifted the particle size distribution toward larger diameter. This graph corroborates the hypothesis of the aggregation of nanoparticles due to the large amount of particles present inside the ablation cell and additionally these results suggest that, under the selected experimental conditions, agglomerates are not collected on the stages of their corresponding primary particles but in a bigger range in contrast to the results reported by Koch et al. [36,42]. This is likely due to the much higher aerosol density of polyacrylamide gels produced by our laser ablation strategy which is 3 to 4 orders of magnitude higher than those used in previous works. In this work, ablation rates were in the range of 1×10^{-3}–7×10^{-3} mm^3 s^{-1} for polyacrylamide gels compared to 8×10^{-7}–3.2×10^{-6} mm^3 s^{-1} for glasses or metals as reported by Gonzalez et al. [33,34]. In addition, ablations of polyacrylamide gels were performed for various lane widths keeping the

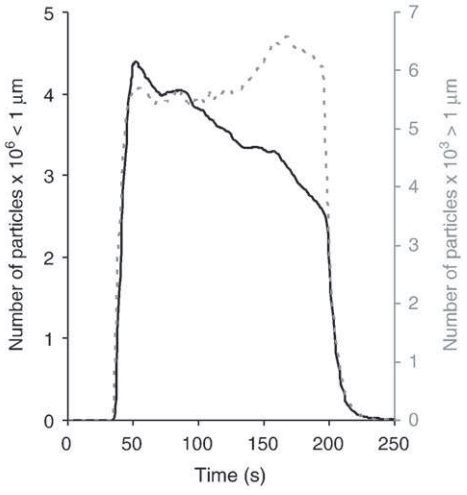

Fig. 4. Real time particle number obtained for the reference femtosecond ablation with the low-pressure impactor.

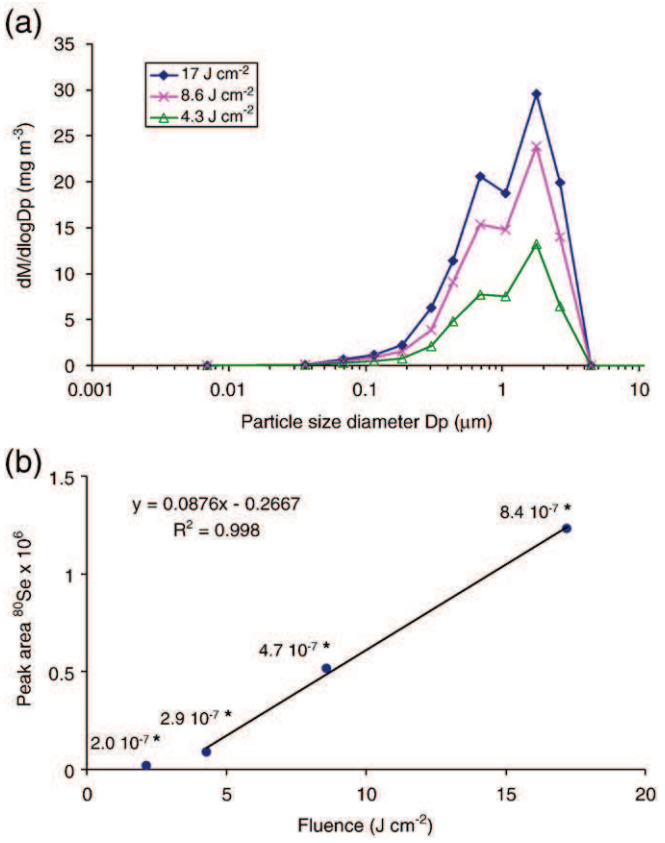

Fig. 5. Effect of the fluence parameter on the femtosecond laser generated aerosol of polyacrylamide gels (reference femtosecond ablation). a) Particle size distribution in mass and b) ^{80}Se ICPMS signal. *Average ablation rate per pulse expressed in mm^3/pulse.

ablation depth constant (Table 2). As shown in Fig. 2, similar trends were observed for the five lanes investigated and the number of smaller particles dropping with the increase of the ablated area, probably because of an intensification of the collisions of tiny particles. Based on the ICPMS signal drop after ablation, the washout time of the ablation cell was measured to be in the range of 23 s for a 90% signal drop and in the range of 53 s for a 99% signal drop. In these conditions, the probability of condensation is obviously increased. A solution to avoid this important aerosol density in the ablation cell could be the use of a short washout ablation cell, as it has been recently proposed by Garcia et al. [29]. However, this kind of ablation cell design demonstrated a poor repeatability, which could be a critical parameter for the development of accurate and precise quantitative methods of analysis. The HEAD (high efficiency aerosol dispersion) ablation cell designed by Pisonero et al. [44] could be a better solution as it permits to reduce the formation of agglomerates.

Finally, another explanation could be the use of the high repetition rate. Fernandez et al. [40], who worked also at 10 kHz, reported that the agglomerates coming from the femtosecond ablation of soils and sediments were not collected on their primary particle size by the low-pressure impactor. Moreover, it can be highlighted that the drop of current signals of smaller particles showed on the reference femtosecond ablation (Fig. 4) appears particularly for the high repetition rate ablation and the high ablation rate. Thus, the formation of aggregates is not only due to the ablation rate but also to the time between one pulse and the other. Indeed, if pulses are close, the particles have not enough time to expand before getting in touch and therefore they tend to stick to each other and agglomerate. In this study, the time difference between one laser pulse and the other (100 µs) corresponds to a shift of 10 µm in the gel. Taking into account these values and the analysis of the temporal progression of expansion of the

aerosol in helium shown by Koch et al. [31], it is highly likely that the aerosol of the first pulse still remains close to the surface before a second pulse occurs. Therefore the collision between the particles ablated by one pulse and the following one are more probable.

Thus, the high aerosol density and the close pulse-to-pulse ablation increased the probability of aggregation. Consequently, the ablated particles were not found at the impactor stage corresponding to fine particles (primary particles of the aggregates) but at that characteristic of larger agglomerates. The ease of disintegration of agglomerates in the ICPMS was investigated further on.

3.1.3. Effect of the fluence

Fluence is one of the key parameters influencing the ablation rate and as a result may induce changes in the characteristics of the generated aerosol. In order to study the influence of this parameter on the particle size distribution, four different fluence values in the range of 2.2 to 17 J cm^{-2} were investigated by using the "reference femtosecond ablation" strategy. In agreement with previously reported observations [27,45], the ablation rate was found to be proportional to the fluence (results not shown). Moreover, as shown in Fig. 5a, the amount of particles increased with the fluence although the particle size distribution was very similar whatever the fluence applied (the lower signal gave a poor signal with the ELPI). These results were in agreement with those reported by Jeong et al. [9] for the analysis of glass samples.

In addition, LA-ICPMS measurements were performed for each of the fluence values studied. The transient signal was recorded when the selenoprotein was ablated and integrated (peak area). As it can be clearly seen in Fig. 5b, the signal detected was proportional to the fluence from 4 to 17 J cm^{-2} which is in good agreement with our previous observation where the ablation rate was proportional to the fluence. However, lower fluences (close to the ablation threshold) did not follow the same linear trend, indicating different processes as previously described by Margetic et al. [46].

3.2. Morphology of the transported aerosol

The size and morphology of the produced particles was evaluated. The laser generated aerosol was collected on filters and analyzed using a scanning electron microscope. It is worth noticing that when stored under ambient conditions, these fine particles rapidly swelled up with ambient humidity due to the hydrophilic nature of the polyacrylamide gels, showing a melted aspect clearly identified by SEM. Special care was then required for a correct observation of such particles. And therefore, in order to keep the particle morphology unchanged, the filters were immediately stored after sampling in the presence of silica gel, under argon, until their introduction into the SEM coating unit. The particle collection time was the same for each ablation in order to compare the amount of material sampled.

Fig. 6 shows typical SEM images of the collected aerosol particles obtained for polyacrylamide gels using femtosecond laser ablation. For 0.12-mm wide lane ablation, only a few particles were found on the filter, whereas the 2-mm wide lane ablation provided much higher particles density made of large agglomerates. While the SEM images cannot be used to provide quantitative information about particle size distribution due to the non-uniform distribution of particles on filter surface, they reveal the shape and texture of the particles which provide crucial information about particle formation processes. It was observed that the agglomerates (in the range of several micrometers) were composed of particles of 100 nm or lower.

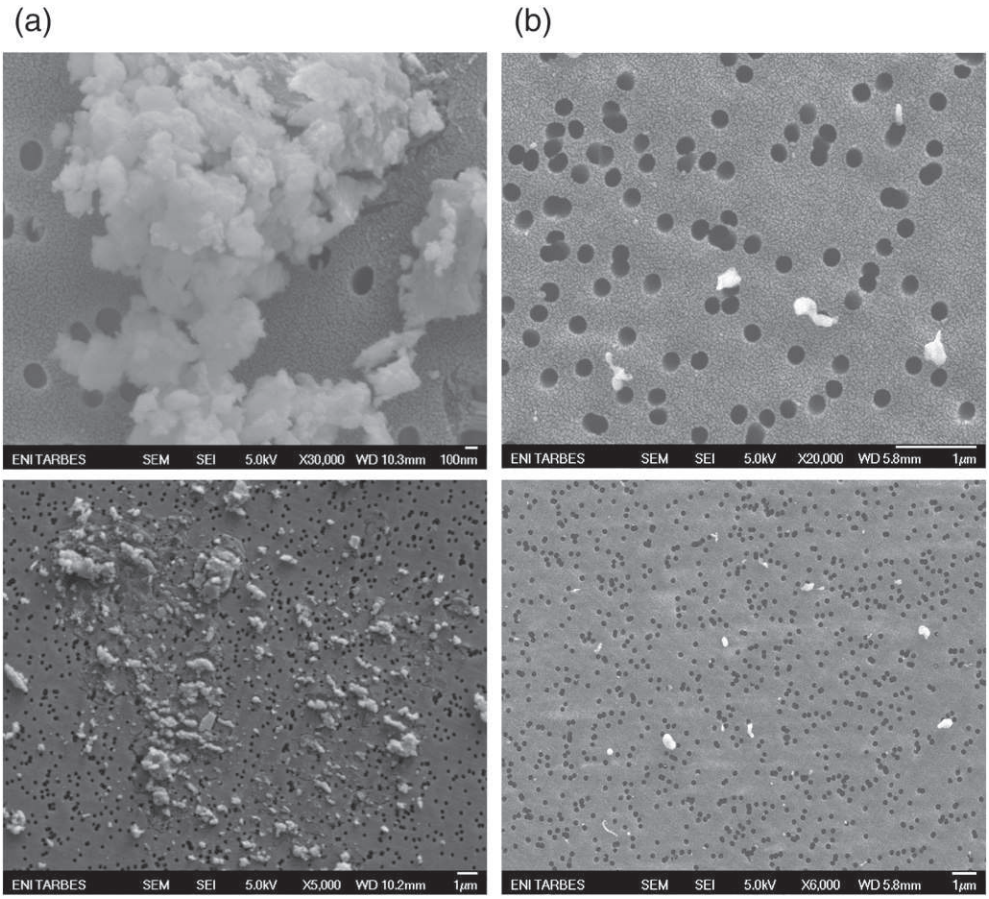

Fig. 6. Scanning electron microscope (SEM) images of the collected aerosol particles produced by (a) the reference femtosecond ablation and (b) a 0.12-mm wide lane femtosecond ablation at 10 kHz with top picture and bottom picture respectively zoom and enlarged views.

3.3. Plasma loading effect: temperature changes

Plasma loading effects were recently studied by Koch et al. [8] to examine the impact of the amount of particles introduced into the ICP on the accuracy of the results. A great change of temperature caused by the plasma loading was found to affect preferentially elements with higher ionization potential and thus, to provoke fractionation because of the difference of ionization potential between elements. As in this work, only one element (selenium) was studied and calibration was performed using similar matrices, fractionation was not a critical benchmark to take into account. Plasma temperature changes were studied in order to investigate the impact of the rather important particle loading on the ICP ionization efficiency. For this purpose, analyses were performed by ablating gels while nebulizing a standard solution containing two elements with different ionization energy. As has been previously shown by O'Connor et al. [47], a wet plasma is much tolerant of increased sample loading without reducing plasma robustness and, therefore, an ultrasonic nebuliser (USN) was used to keep similar dry plasma conditions compared to the routine analysis of polyacrylamide gels.

Then, Ga and Ge were chosen as thermometric elements taking into account the impurities present on the gels and they were introduced using a USN. These elements were associated with respect to their ionization energy (579 kJ mol^{-1} and 762 kJ mol^{-1} respectively) and their close atomic number ($\Delta = 1$ uma). The same simplified Saha equation used by Koch et al. [8] was employed to calculate the temperature difference ΔT:

$$\Delta T = N_a k T^2 \times \frac{ln[R_1 / R_2]}{I_{Ge} - I_{Ga}}$$

where N_a is Avogadro's number, k is Boltzmann's constant, T the temperature of the ICP without loading, I the ionisation energy of Ge which is more difficult to ionize than Ga, and R_1 and R_2 the $^{72}Ge/^{71}Ga$ response ratio for the minimum and the maximum mass loading respectively.

Fig. 7a and b shows the ratio of the thermometric elements obtained when the multielemental solution was introduced at the same time than the ablated aerosol. Two ablation strategies were performed in order to produce different aerosols: a 0.12-mm wide lane ablation at 10 kHz (7a) and the femtosecond reference ablation (7b). A ratio of 0.365 was found without ablation or with a 0.12-mm wide lane ablation whereas a ratio 0.361 was found for the reference femtosecond ablation. Therefore, it can be stated that no significant changes were found and the calculated decrease on plasma temperature was about 25 ± 5 K (from the mean of 3 replicates). This suggests that the cohesion forces between the thin particles composing the large aggregates of the aerosol of polyacrylamide gels are weak enough to have negligible impact on the ICPMS detection.

In addition, the ICPMS signal intensity (peak area) was measured for different particle mass loadings determined by the ELPI for various ablation lanes at 10 kHz (results not shown). The intensity increased linearly with the amount of particles introduced into the plasma suggesting neither matrix effect nor significant plasma loading altered the plasma robustness. The fact that the particle size distribution was shifted toward bigger particles when the particle density increased, suggests that these large particles were easily atomized in the plasma. This result corroborates the previous observation of a very low plasma temperature change as a function of the amount of polyacrylamide particles introduced.

These studies demonstrated that the presence of aggregates and the large amount of particles brought to the ICPMS have very limited negative effects on the Se detection. This may be due to the fact that the fine particles are agglomerated by weak interactions such as e.g. van der Waals forces or ionic/covalent bonds, and then such particles have no significant impact on the ICP source efficiency.

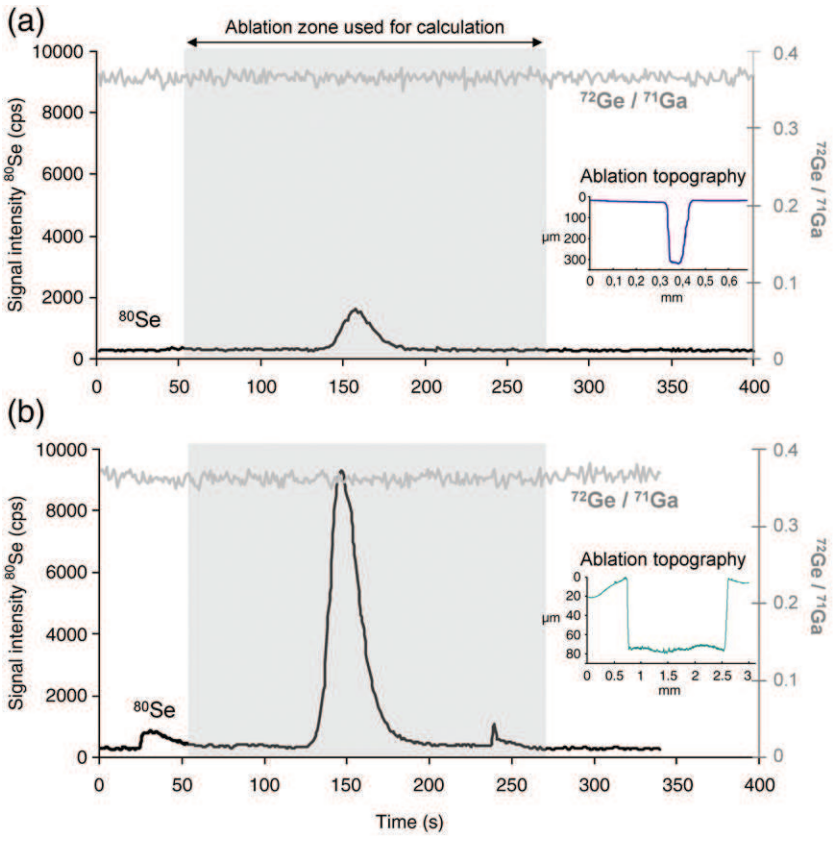

Fig. 7. ^{80}Se ICPMS signal and $^{72}Ge/^{71}Ga$ ratio for (a) a femtosecond ablation of 0.12-mm wide lane at 10 kHz and (b) a femtosecond ablation of 2-mm wide lane at 10 kHz (reference femtosecond ablation). The inset represents the topography of the considered ablation measured by profilometry.

3.4. Calibration curves

Two LA-ICPMS calibrations were performed on gel samples with different selenoprotein concentrations in order to compare the two ablation strategies: the reference femtosecond ablation and a 0.5-mm wide lane ablation performed at 10 kHz. A linear trend was obtained for both strategies between 0 and 400 ng g^{-1} ($y = 12\,824\times + 12\,481$ with $R^2 = 0.9994$; and $y = 3690.4\times + 1\ 697.3$ with $R^2 = 0.9988$ for 2-mm and 0.5-mm wide lanes respectively). However, a factor of 3.5 was found between slopes while the ablation rate differed by a factor of 1.9. This loss of sensitivity could be due to the depth of the 0.5-mm wide lane ablation. Indeed, this strategy is able to remove all the selenoprotein from the gel as its ablation depth corresponds to the thickness of the gel (200 µm). However, as the drying stage of the gel is not controlled enough to obtain a constant thickness all along the gel, the amount of gel ablated could be overestimated. Finally, the particle mass loading measured by the ELPI shows a factor of 3.7 between the two ablation strategies, which is quite similar with the factor found between the slopes of the calibration curves. This demonstrates a lower transport efficiency of the particles coming from the deeper ablation and even if the particle size distribution shows smaller particles for the deeper ablation, the extraction of the aerosol from high depths alter the sensitivity of the analytical method. Therefore, the 2-mm wide lane ablation seems to be the best strategy for the determination of selenoproteins in gel electrophoresis.

4. Conclusions

The characteristics of the aerosols produced by high repetition rate IR femtosecond laser ablation were investigated in terms of particle size distribution, with a low-pressure impactor, and morphology by the use of scanning electron microscopy. This study revealed that this laser generated aerosol was composed of thin particles aggregated into micrometric agglomerates which were formed into the plasma plume and during the transport toward the ICPMS. The formation of these aggregates was facilitated by the high ablation rate and the high repetition rate employed which increases the collision probability between particles. In this sense, ablations of narrow lanes at high repetition rate showed important proportion of thin particles (up to 77% in mass of particles below 1 µm) but demonstrated a lower transport efficiency of the particles coming from the deepest ablation. Moreover, fluence was not found to influence the particle size distribution but permitted to increase the amount of particles ablated. Finally, 2-mm wide lane ablation was demonstrated to be suitable for sampling as it permitted to bring sufficient amount of material without affecting significantly the ICP ionization efficiency. Neither significant plasma temperature changes nor matrix effect could be detected. As a consequence, the detection limit was improved. The signal sensitivity improvement between our 2D high repetition rate femtosecond laser ablation (2-mm wide lane) and the more conventional nanosecond ablation (0.12-mm wide lane) can therefore be partly attributed to the characteristics of the aerosol. Further studies should be carried out to evaluate the transport efficiency which could be responsible for the sensitivity improvement between both laser ablation strategies. Furthermore, the role of the large amount of carbon introduced into the ICP under high repetition rate conditions might be an additional route explaining selenium signal response enhancement [48] that will be considered in further studies.

References

[1] J. Szpunar, Bio-inorganic speciation analysis by hyphenated techniques, Analyst 125 (2000) 963–988.

[2] R. Ma, C.W. McLeod, K. Tomlinson, R.K. Poole, Speciation of protein-bound trace elements by gel electrophoresis and atomic spectrometry, Electrophoresis 25 (2004) 2469–2477.

[3] R. Westermeier, R. Marouga, Protein detection methods in proteomics research, Biosci. Rep. 25 (2005) 19–32.

[4] J.L. Neilsen, A. Abildtrup, J. Christensen, P. Watson, A. Cox, C.W. McLeod, Laser ablation inductively coupled plasma-mass spectrometry in combination with gel electrophoresis: a new strategy for speciation of metal binding serum proteins, Spectrochim. Acta Part B 53 (1998) 339–345.

[5] G. Ballihaut, F. Claverie, C. Pécheyran, S. Mounicou, R. Grimaud, R. Lobinski, Sensitive detection of selenoproteins in gel electrophoresis by high repetition rate femtosecond laser ablation-inductively coupled plasma mass spectrometry, Anal. Chem. 79 (2007) 6874–6880.

[6] J. Gonzalez, S.H. Dundas, C.Y. Liu, X. Mao, R.E. Russo, UV-femtosecond and nanosecond laser ablation-ICP-MS: internal and external repeatability, J. Anal. At. Spectrom. 21 (2006) 778–784.

[7] B. Fernandez, F. Claverie, C. Pécheyran, O.F.X. Donard, F. Claverie, Direct analysis of solid samples by fs-LA-ICP-MS, TrAC, Trends Anal. Chem. 26 (2007) 951–966.

[8] J. Koch, M. Wälle, J. Pisonero, D. Günther, Performance characteristics of ultraviolet femtosecond laser ablation inductively coupled plasma mass spectrometry at 265 and 200 nm, J. Anal. At. Spectrom. 21 (2006) 932–940.

[9] S.H. Jeong, O.V. Borisov, J.H. Yoo, X.L. Mao, R.E. Russo, Effects of particle size distribution on inductively coupled plasma mass spectrometry signal intensity during laser ablation of glass samples, Anal. Chem. 71 (1999) 5123–5130.

[10] S.E. Jackson, D. Günther, The nature and sources of laser induced isotopic fractionation in laser ablation-multicollector-inductively coupled plasma-mass spectrometry, J. Anal. At. Spectrom. 18 (2003) 205–212.

[11] N.J. Saetveit, S.J. Bajic, D.P. Baldwin, R.S. Houk, Influence of particle size on fractionation with nanosecond and femtosecond laser ablation in brass by online differential mobility analysis and inductively coupled plasma mass spectrometry, J. Anal. At. Spectrom. 23 (2007) 54–61.

[12] D.C. Perdian, S.J. Bajic, D.P. Baldwin, R.S. Houk, Time-resolved studies of particle effects in laser ablation inductively coupled plasma-mass spectrometry: Part 1. Investigation of nanosecond and femtosecond pulse width lasers and devices for particle size selection, J. Anal. At. Spectrom. 23 (2008) 325–335.

[13] J. Koch, M. Wälle, R. Dietiker, D. Günther, Analysis of laser-produced aerosols by inductively coupled plasma mass spectrometry: transport phenomena and elemental fractionation, Anal. Chem. 80 (2008) 915–921.

[14] M. Guillong, D. Günther, Effect of particle size distribution on ICP-induced elemental fractionation in laser ablation-inductively coupled plasma-mass spectrometry, J. Anal. At. Spectrom. 17 (2002) 831–837.

[15] B. Hattendorf, C. Latkoczy, D. Günther, Laser ablation-ICPMS, Anal. Chem. 75 (2003) 341A–347A.

[16] M. Guillong, H.R. Kuhn, D. Günther, Application of a particle separation device to reduce inductively coupled plasma-enhanced elemental fractionation in laser ablation-inductively coupled plasma-mass spectrometry, Spectrochim. Acta Part B 58 (2003) 211–220.

[17] H.R. Kuhn, M. Guillong, D. Günther, Size-related vaporisation and ionisation of laser-induced glass particles in the inductively coupled plasma, Anal. Bioanal. Chem. 378 (2004) 1069–1074.

[18] C.Y. Liu, X.L. Mao, J. Gonzalez, R.E. Russo, Study of particle size influence on laser ablation inductively coupled plasma mass spectrometry using an in-line cascade impactor, J. Anal. At. Spectrom. 20 (2005) 200–203.

[19] H.R. Kuhn, D. Günther, The agglomeration state of nanosecond laser-generated aerosol particles entering the ICP, Anal. Bioanal. Chem. 383 (2005) 434–441.

[20] M. Guillong, I. Horn, D. Günther, A comparison of 266 nm, 213 nm and 193 nm produced from a single solid state Nd:YAG laser for laser ablation ICP-MS, J. Anal. At. Spectrom. 18 (2003) 1224–1230.

[21] O. Samek, V. Margetic, R. Hergenröder, Sampling of material using femtosecond pulses, Anal. Bioanal. Chem. 381 (2005) 54–56.

[22] R. Hergenröder, O. Samek, V. Hommes, Femtosecond laser ablation elemental mass spectrometry, Mass Spectrom. Rev. 25 (2006) 551–572.

[23] C. Liu, X.L. Mao, S.S. Mao, X. Zeng, R. Greif, R.E. Russo, Nanosecond and femtosecond laser ablation of brass: particulate and icpms measurements, Anal. Chem. 76 (2004) 379–383.

[24] R. Hergenröder, Laser-generated aerosols in laser ablation for inductively coupled plasma spectrometry, Spectrochim. Acta Part B 61 (2006) 284–300.

[25] Z. Wang, B. Hattendorf, D. Günther, Analyte response in laser ablation inductively coupled plasma mass spectrometry, J. Am. Soc. Mass Spectrom. 17 (2006) 641–651.

[26] D. Günther, C.A. Heinrich, Enhanced sensitivity in laser ablation-ICP mass spectrometry using helium-argon mixtures as aerosol carrier, J. Anal. At. Spectrom. 14 (1999) 1363–1368.

[27] I. Horn, D. Günther, The influence of ablation carrier gasses Ar, He and Ne on the particle size distribution and transport efficiencies of laser ablation-induced aerosols: implications for LA-ICP-MS, Appl. Surf. Sci. 207 (2003) 144–157.

[28] D. Bleiner, D. Günther, Theoretical description and experimental observation of aerosol transport processes in laser ablation inductively coupled plasma mass spectrometry, J. Anal. At. Spectrom. 16 (2001) 449–456.

[29] C.C. Garcia, H. Lindner, K. Niemax, Transport efficiency in femtosecond laser ablation inductively coupled plasma mass spectrometry applying ablation cells with short and long washout times, Spectrochim. Acta Part B 62 (2007) 13–19.

[30] J. Koch, I. Feldmann, N. Jakubowski, K. Niemax, Elemental composition of laser ablation aerosol particles deposited in the transport tube to an ICP, Spectrochim. Acta Part B 57 (2002) 975–985.

[31] J. Koch, S. Schlamp, T. Rosgen, D. Fliegel, D. Günther, Visualization of aerosol particles generated by near infrared nano- and femtosecond laser ablation, Spectrochim. Acta Part B 62 (2007) 20–29.

[32] J. Koch, M. Wälle, S. Schlamp, T. Rosgen, D. Günther, Expansion phenomena of aerosols generated by laser ablation under helium and argon atmosphere, Spectrochim. Acta Part B 63 (2008) 37–41.
[33] J.J. Gonzalez, C. Liu, S.B. Wen, X. Mao, R.E. Russo, Metal particles produced by laser ablation for ICP-MS measurements, Talanta 73 (2007) 567–576.
[34] J.J. Gonzalez, C. Liu, S.B. Wen, X. Mao, R.E. Russo, Glass particles produced by laser ablation for ICP-MS measurements, Talanta 73 (2007) 577–582.
[35] I. Kroslakova, D. Günther, Elemental fractionation in laser ablation-inductively coupled plasma-mass spectrometry: evidence for mass load induced matrix effects in the ICP during ablation of a silicate glass, J. Anal. At. Spectrom. 22 (2007) 51–62.
[36] J. Koch, H. Lindner, A. Von Bohlen, R. Hergenröder, K. Niemax, Elemental fractionation of dielectric aerosols produced by near-infrared femtosecond laser ablation of silicate glasses, J. Anal. At. Spectrom. 20 (2005) 901–906.
[37] J. Koch, A. Von Bohlen, R. Hergenröder, K. Niemax, Particle size distributions and compositions of aerosols produced by near-IR femto- and nanosecond laser ablation of brass, J. Anal. At. Spectrom. 19 (2004) 267–272.
[38] C. Pécheyran, S. Cany, O.F.X. Donard, Ablation laser femtoseconde à haute cadence de tir et basse énergie couplée à une détection ICPMS: Résultats préliminaires, Can. J. Anal. Sci. Spectrosc. 50 (2005) 228–239.
[39] B. Fernandez, F. Claverie, C. Pécheyran, O.F.X. Donard, Solid-spiking isotope dilution laser ablation ICP-MS for the direct and simultaneous determination of trace elements in soils and sediments, J. Anal. At. Spectrom. 23 (2008) 367–377.
[40] B. Fernandez, F. Claverie, C. Pécheyran, J. Alexis, O.F.X. Donard, Direct Determination of trace elements in powdered samples by in-cell isotope dilution femtosecond laser ablation ICP-MS, Anal. Chem. 80 (2008) 6981–6994.
[41] G. Ballihaut, S. Mounicou, R. Lobinski, Multitechnique mass-spectrometric approach for the detection of bovine glutathione peroxidase selenoprotein: focus on the selenopeptide, Anal. Bioanal. Chem. 388 (2007) 585–591.
[42] H.R. Kuhn, J. Koch, R. Hergenröder, K. Niemax, M. Kalberer, D. Günther, Evaluation of different techniques for particle size distribution measurements on laser-generated aerosols, J. Anal. At. Spectrom. 20 (2005) 894–900.
[43] V. Mozna, J. Pisonero, M. Hola, V. Kanicky, D. Günther, Quantitative analysis of Fe-based samples using ultraviolet nanosecond and femtosecond laser ablation-ICP-MS, J. Anal. At. Spectrom. 21 (2006) 1194–1201.
[44] J. Pisonero, D. Fliegel, D. Günther, High efficiency aerosol dispersion cell for laser ablation-ICP-MS, J. Anal. At. Spectrom. 21 (2006) 922–931.
[45] R.E. Russo, Xianglei Mao, J.J. Gonzalez, S.S. Mao, Femtosecond laser ablation ICP-MS, J. Anal. At. Spectrom. 17 (2002) 1072–1075.
[46] V. Margetic, K. Niemax, R. Hergenröder, Application of femtosecond laser ablation time-of-flight mass spectrometry to in-depth multilayer analysis, Anal. Chem. 75 (2003) 3435–3439.
[47] C. O'Connor, B.L. Sharp, P. Evans, On-line additions of aqueous standards for calibration of laser ablation inductively coupled plasma mass spectrometry: theory and comparison of wet and dry plasma conditions, J. Anal. At. Spectrom. 21 (2006) 556–565.
[48] E.H. Larsen, S. Stürup, Carbon-enhanced inductively coupled plasma mass spectrometric detection of arsenic and selenium and its application to arsenic speciation, J. Anal. At. Spectrom. 9 (1994) 1099–1105.